Chapter 4
In-Situ Heating TEM

Shijian Zheng and Longbing He

4.1 A Brief History of In-Situ Heating TEM

In the past, people could only obtain static information from the sample, but advancing science and technology make it possible to apply in-situ stimuli and observe the real-time response. Microheaters allow samples to be thermally stimulated and research on dynamic properties (such as phase transitions, materials growth, sublimation, and catalysis) to rise.

The first likely dynamic STEM observation of the motion of atoms on the surface of thin substrates was reported by Crewe in 1979 [1]. The movement of clusters/atoms and the nucleation process have been observed over periods of several hours. This phenomenon was ascribed to thermal effects and inspired further development of technology to improve the contrast and resolution. Soon after, the first in-situ HRTEM imaging of dislocation formation, motion, interaction, and annihilation in gold due to electron beam irradiation was carried out using a TV system by Hashimoto et al. [2]. A more convincing example of atomic movement caused by heating from an incident electron beam was reported by Sinclair et al. [3]. They captured moving species within the crystal structure of the parent material (CdTe) rather than single atomic jumps and the motion rate became higher with longer exposure (Fig. 4.1). When the beam current density was reduced, the response of the motion rate was slow, which implied that this motion did not result from direct electron-atom collisions or

S. Zheng
Tianjin Key Laboratory of Materials Laminating Fabrication and Interface Control Technology, School of Materials Science and Engineering, Hebei University of Technology, Tianjin 300130, China
e-mail: sjzheng@hebut.edu.cn

L. He (✉)
Key Lab of MEMS of Ministry of Education, SEU-FEI Nano-Pico Center, Southeast University, Nanjing 210096, China
e-mail: helongbing@seu.edu.cn

L. Sun et al. (eds.), *In-Situ Transmission Electron Microscopy*,
https://doi.org/10.1007/978-981-19-6845-7_4

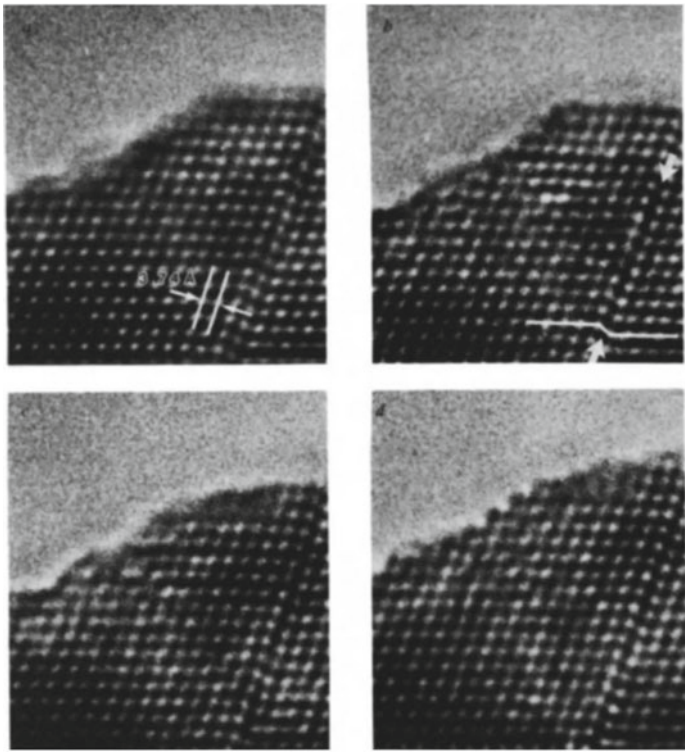

Fig. 4.1 Atomic motion induced by electron beam heating. Four panels are images captured several minutes apart (reproduced with permission from Ref. [3], Copyright 1981, Springer Nature)

ionization effects but presumably arose due to heating dissipation from the active area.

Increasing demand for controllable elevated temperatures during in-situ observation in TEM stimulated Parker's introduction of commercial heating holders in 1986 [4]. The holders exhibited acceptable mechanical and thermal stability to allow high-resolution imaging during the heating process. Besides, a video-rate recording was also realized to follow the dynamic behavior over long periods of time. To demonstrate the technique, Parker et al. observed silicon re-growth at temperatures between 500 and 800 °C. A silicon thin film with a thickness of 300 nm had been deposited on a sapphire substrate and treated by dual ion-implant and annealing. The corresponding TEM specimens were made using a standard cross-section technique. Heating was implemented with a commercial holder (model number PW 6592), where a platinum pad was heated by an electrical feed-through thus the 3-mm disk sample on it was thermally stimulated. There was a thermocouple attached to the pad to measure the temperature and the reading should be fairly close to the actual temperature due to the high thermal conductivities of sapphire and silicon. Reproducible imaging conditions were carefully controlled to keep any beam heating or other effects at a systematic

error level. In their study, they have found that crystallization and defect reactions in silicon are analogous to their predictions that atoms would rearrange at around 600 °C and this phenomenon is similar to that observed in CdTe by electron beam heating [3]. At this point, it is reasonable to expect an atomic-level investigation of structural transformation in many materials during in-situ heating using a similar strategy.

4.2 Current In-Situ Heating TEM Technologies

4.2.1 Operation Mode

TEM can provide extraordinary imaging capability (sub-angstrom spatial resolution) and acquire diffraction and spectroscopy. It generally operates under either TEM mode or STEM mode. TEM mode corresponds to the application of a parallel electron beam while STEM mode uses a focused, small probe scanning over the sample. In TEM mode, HRTEM images are formed by interference between transmitted and diffracted electron beams (phase contrast), but owing to lens aberrations and sample thickness effects, the interpretation of HRTEM images is complicated. In comparison, the interpretation of the image contrast at STEM mode with a high-angle annular dark-field (HAADF) detector is more straightforward, because it is nearly proportional to Z^2 where Z stands for the atomic number. Z-contrast of HAADF-STEM allows visualization of cation mixing at the atomic scale. Furthermore, the combination of STEM and energy-dispersive x-ray spectroscopy (EDX) or electron energy loss spectroscopy (EELS) can obtain chemical information, such as elemental distribution and oxidation state of the materials simultaneously with capture images [5–7]. However, since the low scanning rates may limit the acquisition of instant change of materials, the majority of in-situ observation during heating is operated under TEM mode rather than STEM mode [8].

4.2.2 Type of Heating Holders

The temperature of the specimen can be elevated by using two kinds of heating holders (Fig. 4.2): a furnace-type heating holder (left) that is designed to use standard TEM grids, or a microfabricated-heater-based holder where a localized area is heated through Joule heating [9]. The furnace-based heating holder has long been commercialized and it enables the sample to be heated up to 1300 °C [10, 11]. Unlike the in-situ mechanical experiments in TEM, achieving the sample heating inside a TEM is much easier. For example, Luo et al. investigated the thermal stability of Ni-based superalloy [12], and Liu et al. successfully attached monodisperse Cu nanoparticles onto carbon nanotubes during in-situ heating in a TEM equipped with

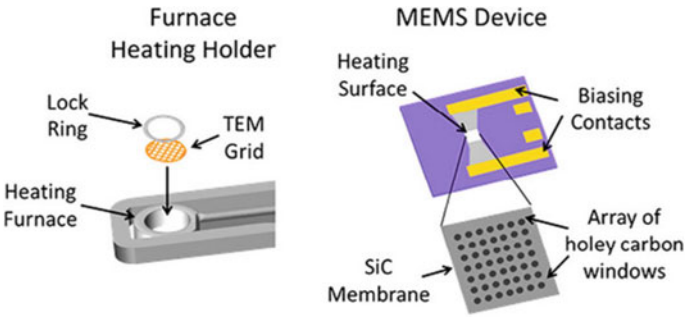

Fig. 4.2 Schematics show two types of heating devices: Furnace heating (left) and MEMS device (right) (reproduced with permission from Ref. [9], Copyright 2018, American Chemical Society)

a Gatan 652 double-tilt heating holder [13]. Nevertheless, the thermal expansion of the stage leads to a non-ignorable image shift during an increase in temperature so it is hard to realize the atomic resolution observation while heating. Especially at temperatures higher than 500 °C, the use of recirculating cooling water to protect the heating unit may also bring vibrations and thereby reduce the imaging stability and resolution. It is challenging to do tests on low-dimensional materials because their morphologies and structures are more sensitive to thermal stimulation. In contrast, the recently developed MEMS-based heating holders only go through negligible mechanical vibrations since heating is localized in a specific small area in the chip and thus allow atomic resolution imaging [14, 15]. For instance, Janish et al. studied nucleation in Ta and captured high-resolution images of nucleating crystallites [16]. In general, the advantage of using furnace-type of holders is that sample preparation is much easier, but the microchip-based holders have better performance regarding temperature control and mitigation of sample drift.

4.2.3 Microheaters

Microheaters are the core of heating holders. The heating zone is usually the region of interest and is placed at the center of the heater since the temperature there is relatively homogeneous. Generally, a microheater includes a silicon substrate or sometimes gallium arsenide and thermally insulating dielectric thin film layers on top [17]. There is an electrically conducting thin film between the substrate and the top insulating layer, where heat is produced by passing electric current provided by the voltage of the current source (This process is called Joule heating). The electrically conducting film can be metal, ceramic or doped polysilicon. Metal is the most frequently used material in microheaters. There are three main reasons. First, since metal has excellent ductility and conductivity, it enables flexible geometrical design and fast response to exerted voltages. Second, due to the near-linear relationship between temperature and resistance, precise temperature control through

resistance measurements can be achieved through a four-point probe. Third, the biggest drawback of metal (i.e. high reaction activity in the environment) can be simply overcome by covering a passivation layer. Ceramic is chemically inert and has high-temperature resistance hence it can be used in tough environments. Doped polysilicon can be easily integrated into standard CMOS processes since it does not limit the following steps as is the issue with metallization [18, 19].

The performance of a microheater is evaluated based on parameters falling into two categories. First, mechanical robustness and stability include mechanical stress, thermal stress, stress distribution, and spatial sample drift. Second, temperature and heat include range and lifetime, homogeneity, accuracy, stability, power consumption, and response time [19].

4.2.4 Synergy with Heating

In addition to single thermal excitation, a combination of heating and other stimuli has shown great potential for research on the dynamic properties of materials in a complicated environment. For example, Karki et al. investigated thermal degradation of overcharged $Li_{0.1}$NCA in different atmospheres using an environmental TEM (ETEM) [20]. Oxidizing, neutral, or reducing environments were created by injecting O_2, He and H_2 gas into the sample area inside the ETEM. They found that surface oxygen loss and structural evolution were inhibited with the oxidizing environment while greatly enhanced under reductive conditions. Moreover, the understanding thermo-electrical performance of materials is also critical to better manipulate and optimize them for practical applications. For instance, it is crucial to monitor structural changes of ReRAM materials while both heating and biasing are applied to improve their stability for the fabrication of future non-volatile memory devices. Hence, Garza et al. [21] present the design of a system for in-situ biasing and heating called Lightning System as shown in Fig. 4.3. The left panel shows the structure of the nanochips for heating and biasing at the same time. There are eight electrical contacts and half of them are used for heating while the other four are used for biasing. This design ensures 4-point probe measurements for accurate control of the temperature and voltage/current which further guarantees a reproducible response. Then, this nanochip is attached to a customized holder (Right panel in Fig. 4.3), where contact needles are used to provide stimuli from outside of the holder. The system can supply voltage up to 100 V and temperature up to 800 °C while it also enables double-tilt during observation. In-situ simultaneous biasing and heating can carve a new path for a comprehensive understanding of materials and advance the development of nano-electronics. Another typical example has been reported by Wang et al., who utilizes the mechanical tests system during increasing the temperature aiming to select the appropriate alloys for aero-engines [22]. Their work also implies that the cooperation among microscopists, physicists, chemists, and engineers is essential for developing next-generation smart materials.

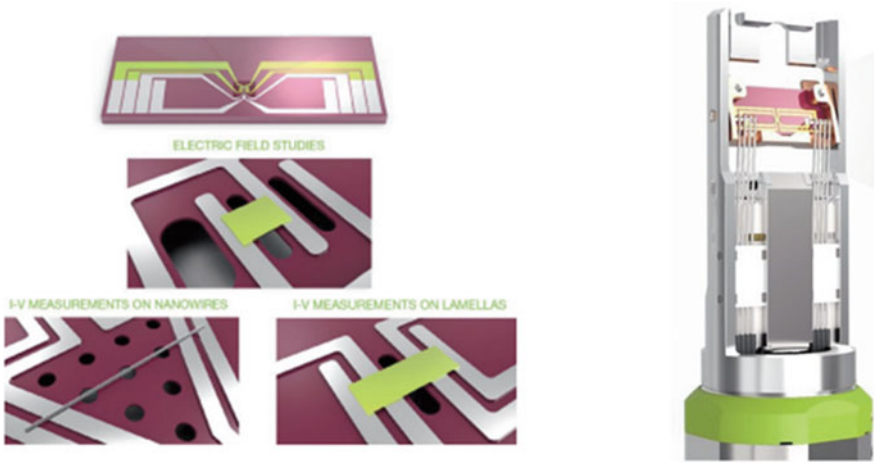

Fig. 4.3 Configuration of nanochip (left) and customized holder with mounted nanochip (right) (reproduced with permission from Ref. [21], Copyright 2016, John Wiley and Sons)

4.3 Research Based on In-Situ Heating TEM

4.3.1 Material Growth

Controllable growth of functional nanomaterials is the starting point for their application in multitudinous devices. Therefore, to explore optimal crystal structures and morphologies, it is necessary to develop methods that can help deeply understand the actual mechanisms behind their growth. The growth of one-dimensional (1D) nanostructures is usually elucidated via a vapor–liquid-solid (VLS) theory. According to the VLS process, the liquid phase dissolves atoms from a solid matrix. When it is supersaturated, growth arises at the surface of the droplet [23]. As the nanostructure is extremely small, a method with a high spatial resolution is crucial to systematically investigate the growth process. The conventional ex-situ observations using microscopy can only analyze the static nanoscale structural information, however, they are incapable of following their forming process [24–26]. By comparison, the in-situ methods enable direct observation of structural transformation occurring at the nanoscale or even atomic scale [27]. For instance, by equipping a heating component, modern TEM can be employed not only for improving resolution but also for making it possible to track dynamic processes during nanowire growth [28, 29], as shown in Fig. 4.4a. During crystal growth, especially in a VLS process, the motion of a semiconductor–metal molten zone is generally motivated by a temperature gradient. Yet, the temperature gradient fields have not been completely understood in earlier ex-situ characterization [30, 31]. Hence, the real-time evidence acquired via in-situ methods provides an opportunity to accurately track liquid zone motion inside the solid [32–34].

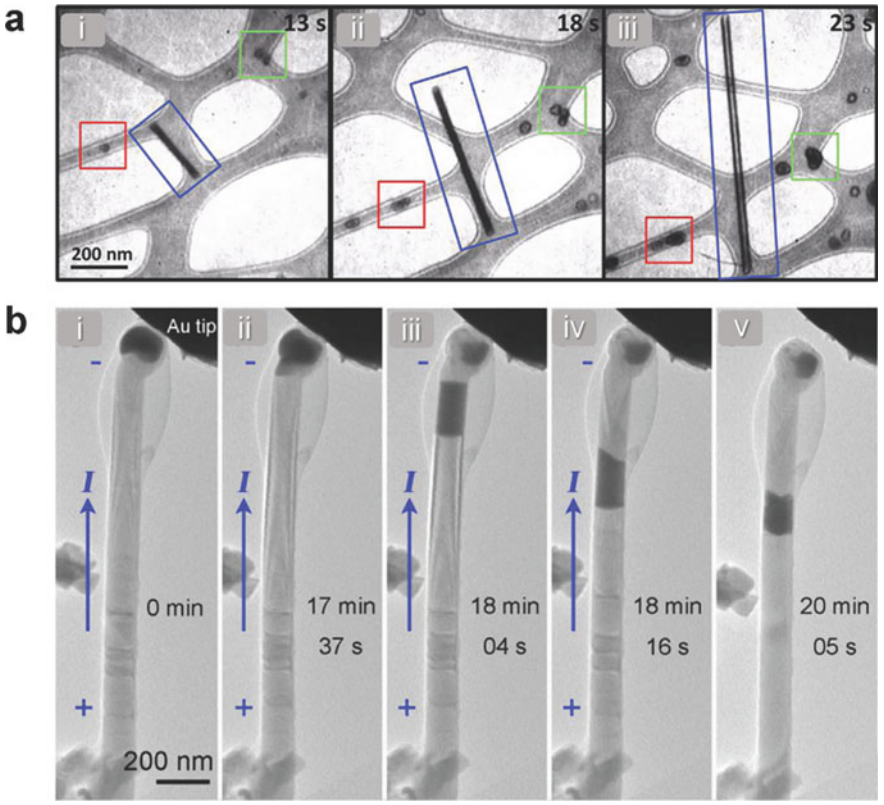

Fig. 4.4 **a** TEM images showing the growth of Cu nanowires during heating (reproduced with permission from Ref. [29], Copyright 2018, American Chemical Society) **b** TEM images exhibiting the motion of Au/Ge alloy during heating (reproduced with permission from Ref. [35], Copyright 2015, American Chemical Society)

Figure 4.4b illustrates an Au particle initially liquifies at the Ge nanowire tip, then creating an Au/Ge alloy liquid area which subsequently moves inside the Ge nanowire [35]. It should be clear that the motion direction and position of the Au/Ge liquid can be manipulated by the applied bias; upon removal of the bias, the Ge nanowire is detached from the Au tip and the liquid Au/Ge alloy quickly hardens. These results resolve the growth kinetics of nanowires, and also inspire more explorations of the growth process of nanoparticles and nanosheets. However, sample handling of them is more complicated. It is expected that a deep investigation of physical and chemical evolutions during material growth at such high resolutions would drive the development of surface and interface engineering.

Later, Cheng et al. found that the growth processes of PbSe nanocrystals (NCs) can be controlled by changing temperature [36]. The NCs begin to grow under the oriented attachment growth mode by attaching dot-shaped NCs along a certain crystal orientation, and sequentially switch to growth with grain-boundary migration

by absorption of smaller NCs by neighboring larger ones through interfacial atom reconstruction.

4.3.2 Sublimation and Surface Energy

Besides crystal growth, sublimation is another important phase transition during which the chemical bonds within the solids break-down resulting in gasification. The in-situ experiment in TEM is a direct technique to investigate the sublimation mode at the atomic scale and it should also shed light on a better understanding of the inverted growth process. Additionally, sublimation is strongly linked to material stability, and the research on sublimation of NCs would reveal the critical factors influencing the stability. For example, though the surface free energies of the major crystal planes follow (111) < (100) < (110) in face-centered cubic (FCC) structures [37, 38], the thermally stable surface of FCC metals at elevated temperatures has been under debate for a long period because high-temperature-induced relaxation of crystal planes strongly depends on crystal index [39–41]. Hence the observation of the stable facets of FCC metals at high temperatures has significant importance for clarifying this debate. Ding et al. [42] and He et al. [43] studied the sublimation scenarios of Ag NCs via in-situ heating TEM. The featured shapes and surfaces during sublimation provide direct information for revealing the close linkage between surface free energy and stability (Fig. 4.5). Benefiting from the low drift of the microchip during heating, the dynamic sublimation process of the Ag NC at the very initial can be effectively captured, showing an overwhelming superiority comparing with the furnace-type heating holder.

Aside from this temperature-related surface stability, in fact, the surface energy of a NC itself is still under fierce debate when taking into account the size effect. Theories and simulations from the thermodynamic view suggest a decreasing trend of surface energy with decreasing particle size [44–46], while another view which considers the size-dependent lattice parameters proposes a rather contrary conclusion [47, 48]. On this issue, the in-situ heating TEM becomes the only effective tool for performing investigations from the experimental end. Sambles et al. probed into the surface energies of Au and Ag NCs by fitting the sublimation curves with Kelvin equation [49, 50]. Later, investigations using similar in-situ heating approach achieved more results for understanding the size effect in surface energy [51]. Although the current in-situ heating TEM still cannot clarify all the inconsistencies remained, the development of more delicate microchips with high controllability and accuracy can provide opportunities for modifying/calibrating the physical parameters of nanomaterials.

In addition to the surface energy, the particle size and defects are also of great importance, which further affects the stability of the nanostructure. Cheng et al. discussed the sublimation process of PbSe nanocrystals at the atomic scale and corresponding size, surface, and interface effects [52]. Because of the interplay between the electron beam and surface organic ligands, the sizes of nanocrystals

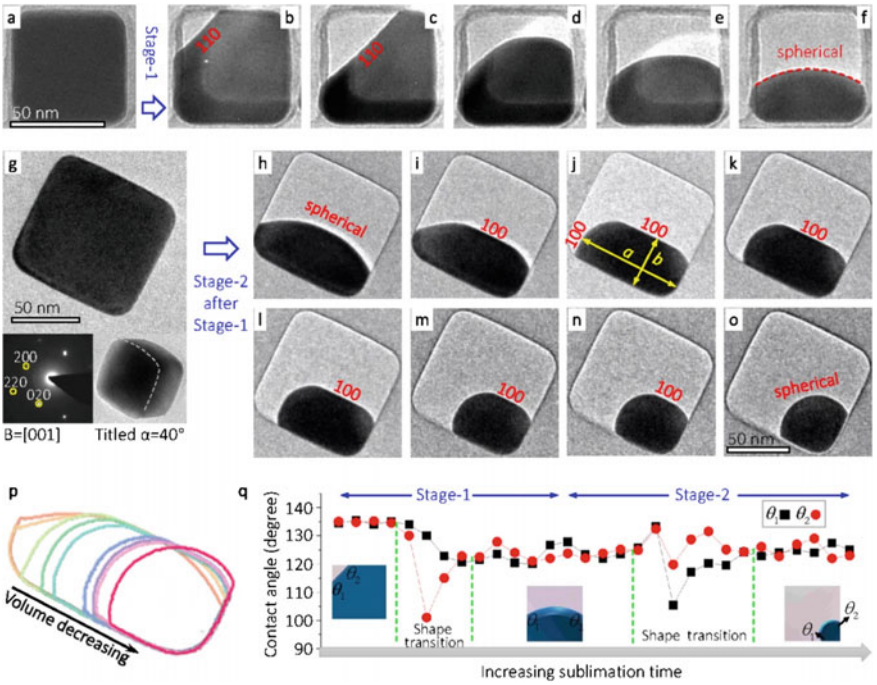

Fig. 4.5 TEM image sequences showing the surface evolution of a cubic Ag NC with a carbon shell (reproduced with permission from Ref. [43], Copyright 2017, John Wiley and Sons)

are successfully manipulated via the introduction of the electron beam at different growth periods, which allows real-time observation of the size dependence of sublimation. As shown in Fig. 4.6, the nanoparticles with a size less than 10 nm exhibit directional orientational sublimation, and those of larger size sublimate uniformly.

4.3.3 Failure Analysis

In in-situ heating TEM, Joule heating is not only used to create a heating region serving as the substrate, but also it is frequently exerted directly in the sample to create synergistic effects. The combination of heat and electromagnetic field frequently leads to unique behaviors in nanomaterials [53]. For example, by controlling the stimulus of atom migration with an appropriate current (i.e. to create a certain temperature and electron-wind force), the mass transport of nano-objects can be implemented at the atomic scale [54–57]. This provides a fantastic method to modulate the nanostructures to enable diverse nanodevices and applications including mass sensors and resonators [58, 59], archival memory [60], oscillators [61], and nano-welding [62]. Aside from these electromigration-based mass transportation phenomena, the

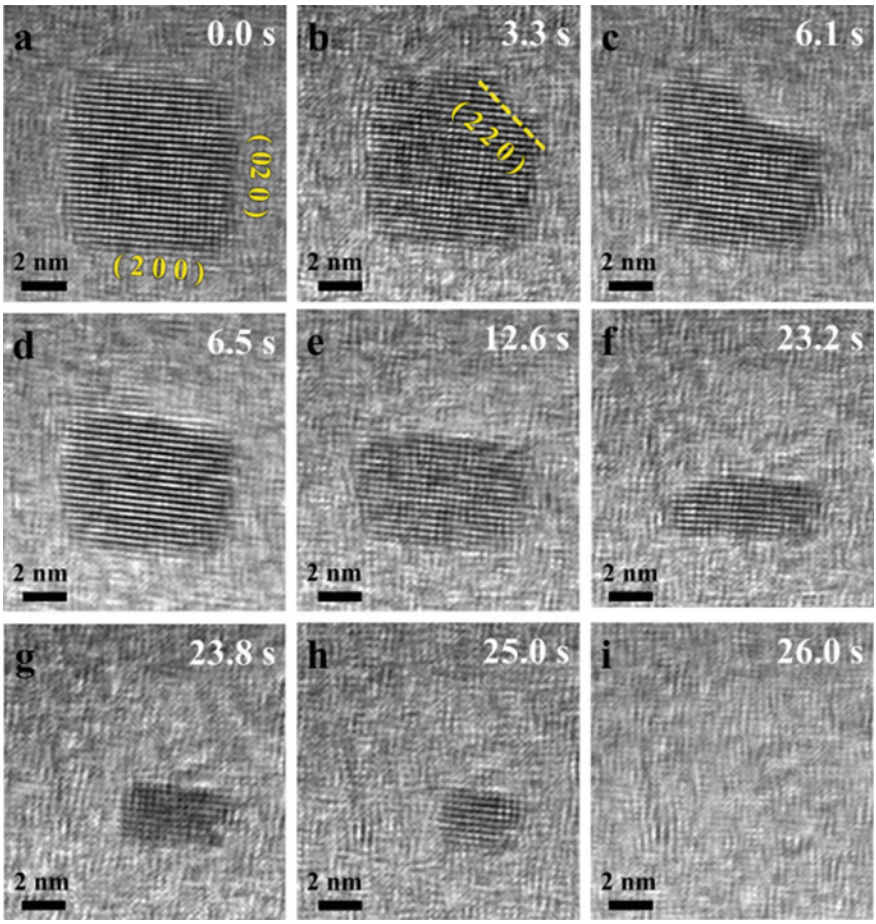

Fig. 4.6 Series of TEM images showing sublimation of a small PbSe nanocube is controlled by its facets (reproduced with permission from Ref. [52], Copyright 2020, Elsevier)

combination of thermal heating with electrical stimuli can also enable ion transport [63–66] and solid-state reactions [67–71]. Mei et al. [72] investigated the solid state reaction/alloying process between nanometer-sized Cu and Al metallic tips. It was found that hetero-joining could be implemented by the coupling of heating and electromigration.

Group III–V nanowires prepared by metal-catalyzed chemical vapor deposition have recently attracted an explosion of interest [73], driven by the inspiring optoelectronic properties, the high crystallinity, and the potential of integrating them with silicon. Recent research on Si nanowires suggests that when the nanowire diameter is below around 150 nm, the thermal conductivity is weakened because of phonon surface scattering [74]. Thermal breakdown in Joule-heated GaN nanowires is studied by in-situ TEM experiment [75]. The thermal conductivity of the nanowires

is reckoned to be below the bulk GaN value. Breakdown in a single nanowire is observed to happen at a maximum temperature of about 1000 K, and nanowire morphology adjacent to the breakdown region suggests that failure happens via thermal decomposition, which is proved by in-situ TEM images captured at the failure stage.

4.3.4 Annealing and Phase Transitions

In-situ annealing provides more dynamic information of sample's structure evolution than the ex-situ approaches. This enables an easy combination between the treating temperatures and the intermediate structures. For example, the FeCrAl alloys are thought to be promising materials of fuel claddings in nuclear reactors. To deeply understand the transformation of helium bubbles and dislocation loops during the annealing process, He^+-irradiated TEM specimens were annealed and characterized by in-situ TEM [76]. The dislocation density reduced with the rise of temperature, but the loop size presented a different behavior. When the temperature was raised to 1072 K, the bubbles grew quickly while the density reduced. Moreover, in-situ thermal annealing of $PtCu_3$/C in TEM has also been studied, which reveals essential transformations for achieving highly-active oxygen reduction [77].

Phase transitions are a well-known temperature-dependent process in materials, in-situ techniques in TEM allow direct observation of these processes [78]. For example, polymorphs of Ga_2O_3 [79] are potential candidates for ultra-wide bandgap semiconductors and are widely studied because of the newly developed growth technologies. The temperature-dependent phase transformation of κ-Ga_2O_3 layers grown on sapphire was investigated by high-resolution TEM [80]. Annealing procedures up to 1000 °C were performed in situ in TEM. This enabled the reveal of the mechanisms of κ-to-β phase transition and corresponding atomic rearrangement.

Likewise, the complex phase diagram of $Pr_{1-x}Ca_xMnO_3$ (PCMO) leads to possibilities of tuning the physical properties for various applications. Significantly, as a result of strong correlation effects, electronic and lattice degrees of freedom are strongly coupled. Therefore, it is arguable whether the bulk phase diagrams can be directly transferred to strained thin films. Beche et al. explored phase transitions at high temperatures in PCMO ($x = 0.1$) deposited as a 400 nm film on a $SrTiO_3$ (STO) substrate [81]. Combination with TEM, individual domains of the nano-twinned films can be resolved compared with macroscopic X-ray or neutron diffraction studies [82].

Recently, Tang et al. [83] investigated the phase evolution of CuAg alloy NCs by in-situ heating TEM. They found that the transition from a solid solution phase to a Janus-type separated phase leads to the formation of different interfaces related to nanoparticle size. Small nanoparticles tend to form a Cu(100)/Ag(100) interface, while the large ones tend to form a Cu(111)/Ag(111) interface. Ni et al. [84] demonstrates that in-situ annealing also helps fine-tune the phase of Au–Ag nanorods to optimize their plasmonic properties. It is interesting that the microchip can also be used as a calibrator to estimate the beam heating effect inside the TEM. In this way,

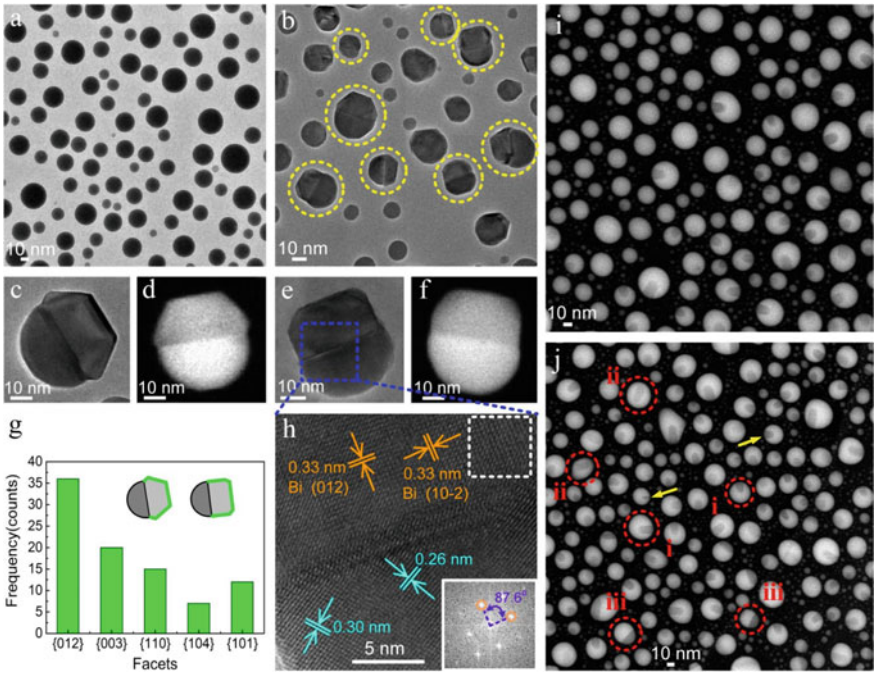

Fig. 4.7 Different morphologies, structures, and phases of PbBi nanoparticles during evolution under in-situ heating treatments (reproduced with permission from Ref. [85] Copyright 2022, American Chemical Society)

the electron beam can be used as an ultra-fast heating source to explore those transient phases that are hardly revealed by conventional methods. Shi et al. [85] used this technique approach to probe into the phase segregation process of PbBi nano-alloy. They have uncovered several metastable phases which haven't been reported before (Fig. 4.7).

4.3.5 Catalysis and Battery

Ordered intermetallic nanoparticles have shown electrocatalysis with improved activity and durability for the oxygen reduction reaction (ORR) [86–88]. Using in-situ heating electron microscopy, morphological evolution and the creation of fully and partially ordered nanocrystals have been observed at the atomic scale [89]. This comprehensive study will have a long-lasting influence on the development of ordered intermetallic electrocatalysts for real-world applications.

Temperature is one of the key factors limiting the application of batteries, thus in-situ heating can be employed to investigate the structural and chemical transformation of battery materials at elevated temperatures. Determining the rational working

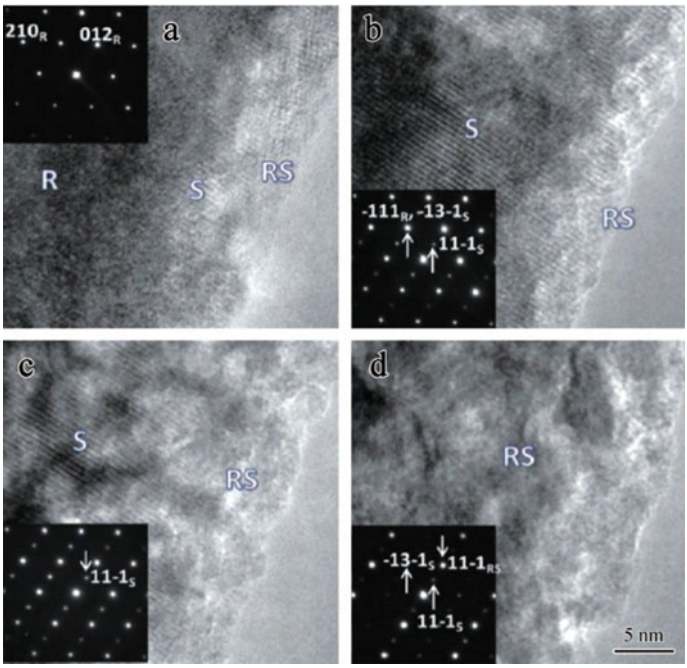

Fig. 4.8 HRTEM images of overcharged nanoparticles: **a** before heating **b** heating at 100 °C **c** heating at 200 °C and **d** heating at 300 °C (reproduced with permission from Ref. [93], Copyright 2013, John Wiley and Sons)

temperature ranges of certain battery materials is critical for developing high-performance batteries to be used in extreme conditons [90–92]. Thermal stability of anode materials may lead to safety issues, so different approaches are demanded to prevent thermal runaway and burning. Nam et al. [93] employed in-situ technologies in TEM to study the thermal stability of overcharged cathode materials, as illustrated in Fig. 4.8. Their work is practically significant since the working temperature is usually changeable rather than constant.

4.3.6 Solid-State Amorphization and Crystallization

One of the most fascinating findings in the 1980s is the formation of amorphous phases by the interplay of two metals at their interfaces [94]. As semiconductor–metal interfaces are vital structures in integrated circuits, Holloway et al. focused on Ti-Si multilayers and discovered that there is also a solid-state amorphization reaction between the interfaces [95]. Additionally, during the early periods of silicidation, an amorphous barrier is formed at the crystalline interface, leading to a high Schottky barrier height [96].

In contrast to amorphization, there is unexpected crystallization observed in some eutectic systems (Al–Si or Ag–Si). In-situ high-resolution TEM reveals that rather than a metastable phase or liquid formation, the initial amorphous phase could be crystallized during adjusting the temperature [97]. Further investigation showed that this crystallization occurred by semiconductor elements diffusing into the metal, then precipitation of the semiconductor would happen after supersaturation [98]. A more thorough research of crystallization in a promising high-k dielectric tantalum oxide enabled a typical Avrami (Kolmogorov– Johnson–Mehl–Avrami) examination of the in-situ experiment. During the observation, the reaction was all the way tracked, thus the nucleation and the growth stages were simply separated for detailed analysis [99].

4.3.7 Degradation of Perovskite Solar Cells

One of the most serious problems limiting the practical application of perovskite solar cells is the lack of thermal stability. Different possible degradation pathways exist in this material system, especially hybrid composites. Therefore, it is inevitable to examine the response of perovskite materials at elevated temperatures. Divitini et al. monitored morphology, structural and chemical changes when heating the prototypes of perovskite solar cells. They present element diffusion and structure break-down and discovered distinct degradation modes in vacuum or air [15].

4.4 Conclusions and Outlook

In summary, in-situ heating TEM plays an increasingly important role in advancing the development of materials for precise structural design and accurate performance control to adapt them to practical applications. In-situ heating offers unique direct information that is not available by other ex-situ methods [100, 101]. In-situ experiments are usually carried out in “TEM mode” to achieve both high spatial resolution and fast recording while “STEM mode” allows more detailed analysis of chemical and electronic information of materials when combined with spectroscopic methods.

However, there are still some issues about in-situ heating in TEM. First, whether the observations are representative of the corresponding bulk materials. Second, the recording rate may still limit the capture of thermally activated processes. Third, data storage and processing capability may affect the in-depth analysis. Fourth, temperature measurement at the microscale remains challenging. Five, it still lacks research on complicated or composite systems, and current studies mainly focus on simple model material systems and reactions.

In the future, in-situ heating TEM should get the following items improved.

Measurement of electron beam effects and their mitigation. High energy electron beam possibly causes destructive changes to the TEM sample and leaves artifacts affecting the objective analysis. Therefore, electron dose, the energy of electrons, vacuum conditions, and nature of materials that determine interaction with the electron beam should be paid careful attention to [102].

High spatial resolution and temporal resolution. Based on more electron-sensitive complementary metal oxide semiconductor, higher special and temporal resolution can be realized, which is crucial for revealing the ultra-fast physical and chemical changes and also for investigating the e-beam irradiation sensitive materials [103]. Scanning rates of probe aberration-corrected STEMs are becoming much faster, so HAADF-STEM in-situ observation is expected to play increasingly vital roles in tracking temperature-dependent processes at the atomic scale. Together with EELS and EDS analysis, local changes in chemical composition and valence states of the elements can be monitored during the increasing/decreasing of the temperature [104].

Rapid data recording and processing. Recently developed faster-recording devices will promote the rate/speed at which changes induced by temperature elevation can be tracked, which will result in an enormous increase in data accumulation. The in-situ experiments at nano-second rates by laser pulsing the electron source will also demand much higher data processing power and artificial intelligence should be one of the feasible solutions [105].

Precise temperature measurement down to microscale or even nanoscale. Although estimation of temperature has been achieved via resistivity measurements [106], more accurate local temperature readouts remain challenging.

Multifunctional holders for simultaneous application of different stimuli. Advancement of versatile in-situ TEM approaches that can offer coupled external stimuli. The structural transformation under multiple external stimuli such as mechanical loading, thermal activation, and electric field, or even in a gas atmosphere [107], liquid environments [108], laser illumination [109, 110], magnetic fields [111, 112] etc., have also been observed nowadays. It is expected that future TEM technologies could incorporate multiple fields that simulate the real working environments for the materials.

Expanding material systems where in-situ heating is employed. It is expected that in-situ heating TEM would continue motivating intriguing discoveries in materials science and further promote industrial development. With the development of advanced unique heating holders combined with the ongoing improvement of the transmission electron microscope, the scope of corresponding in-situ heating studies is only limited by the imagination and innovation of the researcher. It should be believed that much fundamental understanding of material properties will be obtained with an increased resolution both spatially and temporally.

References

1. Crewe AV (1979) Direct imaging of single atoms and molecules using the STEM. Chem Scr 14:17–20
2. Hashimoto H, Takai Y, Yokota Y, Endoh H, Fukada E (1980) Direct observations of the arrangement of atoms around stacking faults and twins in gold crystals and the movement of atoms accompanying their formation and disappearance. Jpn J Appl Phys 19(1):L1–L4. https://doi.org/10.1143/jjap.19.l1
3. Sinclair R, Yamashita T, Ponce FA (1981) Atomic motion on the surface of a cadmium telluride single crystal. Nature 290(5805):386–388. https://doi.org/10.1038/290386a0
4. Sinclair R, Parker MA (1986) High-resolution transmission electron microscopy of silicon re-growth at controlled elevated temperatures. Nature 322(6079):531–533. https://doi.org/10.1038/322531a0
5. Lin F, Markus IM, Nordlund D, Weng T-C, Asta MD, Xin HL, Doeff MM (2014) Surface reconstruction and chemical evolution of stoichiometric layered cathode materials for lithium-ion batteries. Nat Commun 5(1):3529. https://doi.org/10.1038/ncomms4529
6. Gu M, Belharouak I, Genc A, Wang Z, Wang D, Amine K, Gao F, Zhou G, Thevuthasan S, Baer DR, Zhang J-G, Browning ND, Liu J, Wang C (2012) Conflicting roles of nickel in controlling cathode performance in lithium ion batteries. Nano Lett 12(10):5186–5191. https://doi.org/10.1021/nl302249v
7. Kim H, Kim MG, Jeong HY, Nam H, Cho J (2015) A new coating method for alleviating surface degradation of $LiNi_{0.6}Co_{0.2}Mn_{0.2}O_2$ cathode material: nanoscale surface treatment of primary particles. Nano Lett 15(3):2111–2119. https://doi.org/10.1021/acs.nanolett.5b00045
8. Contarato D, Denes P, Doering D, Joseph J, Krieger B (2012) High speed, radiation hard cmos pixel sensors for transmission electron microscopy. Phys Procedia 37:1504–1510. https://doi.org/10.1016/j.phpro.2012.04.103
9. Veghte DP, China S, Weis J, Lin P, Hinks ML, Kovarik L, Nizkorodov SA, Gilles MK, Laskin A (2018) Heating-induced transformations of atmospheric particles: environmental transmission electron microscopy study. Anal Chem 90(16):9761–9768. https://doi.org/10.1021/acs.analchem.8b01410
10. Aradi E, Lewis-Fell J, Harrison RW, Greaves G, Mir AH, Donnelly SE, Hinks JA (2018) Enhanced radiation tolerance of tungsten nanoparticles to He ion irradiation. Nanomaterials 8(12). https://doi.org/10.3390/nano8121052
11. Ipatova I, Harrison RW, Terentyev D, Donnelly SE, Jimenez-Melero E (2017) Thermal evolution of the proton irradiated structure in tungsten–5 wt% tantalum. J Fusion Energy 36(6):234–239. https://doi.org/10.1007/s10894-017-0145-y
12. Sihai L, Xiangfan N, Liucheng Z, Xi Y, Weifeng H, Yinghong L (2017) Thermal stability of surface nanostructure produced by laser shock peening in a Ni-based superalloy. Surf Coat Technol 311:337–343. https://doi.org/10.1016/j.surfcoat.2017.01.031
13. Liu C, Wu S, Zheng H, Cao F, Sheng H, Zhao D, Wang J (2015) Size-controllable fabrication of Cu nanoparticles on carbon nanotubes by simple heating. Mater Res Bull 61:270–274. https://doi.org/10.1016/j.materresbull.2014.10.019
14. Zhang Q, Chang Y, Gu L, Luo Y, Ge B (2017) Study of microstructure of nickel-based superalloys at high temperatures. Scripta Mater 126:55–57. https://doi.org/10.1016/j.scriptamat.2016.08.013
15. Divitini G, Cacovich S, Matteocci F, Cinà L, Di Carlo A, Ducati C (2016) In situ observation of heat-induced degradation of perovskite solar cells. Nat Energy 1(2):15012. https://doi.org/10.1038/nenergy.2015.12
16. Janish MT, Mook WM, Carter CB (2015) Nucleation of fcc Ta when heating thin films. Scripta Mater 96:21–24. https://doi.org/10.1016/j.scriptamat.2014.10.010
17. Hotovy I, Rehacek V, Mika F, Lalinsky T, Hascik S, Vanko G, Drzik M (2008) Gallium arsenide suspended microheater for MEMS sensor arrays. Microsyst Technol 14(4–5):629–635. https://doi.org/10.1007/s00542-007-0470-6

18. Franssila S (2010) Introduction to microfabrication, 2 edn. John Wiley & Sons
19. Spruit RG, Omme JTv, Ghatkesar MK, Garza (2017) A review on development and optimization of microheaters for high-temperature *in situ* studies. J Microelectromech Syst 26(6):1165–1182. https://doi.org/10.1109/jmems.2017.2757402
20. Karki K, Huang Y, Hwang S, Gamalski AD, Whittingham MS, Zhou G, Stach EA (2016) Tuning the Activity of Oxygen in $LiNi_{0.8}Co_{0.15}Al_{0.05}O_2$ battery electrodes. ACS Appl Mater Interfaces 8 (41):27762–27771. https://doi.org/10.1021/acsami.6b09585
21. Pérez Garza HH, Zuo K, Pivak Y, Morsink D, Zakhozheva M, Pen M, van Weperen S, Xu Q MEMS-based system for in-situ biasing and heating solutions inside the TEM. In: European microscopy congress, pp 237–238 (2016). https://doi.org/10.1002/9783527808465.EMC2016.6710
22. Wang J, Lu J, You X, Ullah R, Sang L, Chang L, Zhang Y, Zhang Z (2019) In-situ comparison of deformation behavior at 23 °C and 650 °C of laser direct melting deposited Ti-6Al-4V alloy. Mater Sci Eng, A 749:48–55. https://doi.org/10.1016/j.msea.2019.01.111
23. Joyce HJ, Gao Q, Tan HH, Jagadish C, Kim Y, Fickenscher MA, Perera S, Hoang TB, Smith LM, Jackson HE, Yarrison-Rice JM, Zhang X, Zou J (2009) Unexpected benefits of rapid growth rate for III−V nanowires. Nano Lett 9(2):695–701. https://doi.org/10.1021/nl803182c
24. Jung CS, Kim HS, Im HS, Park K, Park J, Ahn J-P, Yoo SJ, Kim J-G, Kim JN, Shim JH (2015) In situ temperature-dependent transmission electron microscopy studies of pseudobinary $mGeTe{\cdot}Bi_2Te_3$ (m = 3–8) nanowires and first-principles calculations. Nano Lett 15(6):3923–3930. https://doi.org/10.1021/acs.nanolett.5b00755
25. Behafarid F, Pandey S, Diaz RE, Stach EA, Cuenya BR (2014) An in situ transmission electron microscopy study of sintering and redispersion phenomena over size-selected metal nanoparticles: environmental effects. Phys Chem Chem Phys 16(34):18176–18184. https://doi.org/10.1039/c4cp02574a
26. Zhu G, Jiang Y, Lin F, Zhang H, Jin C, Yuan J, Yang D, Zhang Z (2014) In situ study of the growth of two-dimensional palladium dendritic nanostructures using liquid-cell electron microscopy. Chem Commun 50(67):9447–9450. https://doi.org/10.1039/c4cc03500c
27. Zhang Q, Li H, Gan L, Ma Y, Golberg D, Zhai T (2016) In situ fabrication and investigation of nanostructures and nanodevices with a microscope. Chem Soc Rev 45(9):2694–2713. https://doi.org/10.1039/c6cs00161k
28. Boston R, Schnepp Z, Nemoto Y, Sakka Y, Hall Simon R (2014) In situ TEM observation of a microcrucible mechanism of nanowire growth. Science 344(6184):623–626. https://doi.org/10.1126/science.1251594
29. Lin T-Y, Chen Y-L, Chang C-F, Huang G-M, Huang C-W, Hsieh C-Y, Lo Y-C, Lu K-C, Wu W-W, Chen L-J (2018) In situ investigation of defect-free copper nanowire growth. Nano Lett 18(2):778–784. https://doi.org/10.1021/acs.nanolett.7b03992
30. Berg A, Mergenthaler K, Ek M, Pistol M-E, Reine Wallenberg L, Borgström MT (2014) In situetching for control over axial and radial III–V nanowire growth rates using HBr. Nanotechnology 25(50):505601. https://doi.org/10.1088/0957-4484/25/50/505601
31. Aslam Z, Nicholls R, Koós A, Nicolosi V, Grobert N (2011) Current-induced restructuring and chemical modification of N-doped multi-walled carbon nanotubes. Adv Func Mater 21(20):3933–3937. https://doi.org/10.1002/adfm.201101036
32. Ortega Y, Jäger W, Piqueras J, Häussler D, Fernández P (2013) In situTEM and analytical STEM studies of ZnO nanotubes with Sn cores and Sn nanodrops. J Phys D Appl Phys 46(39):395301. https://doi.org/10.1088/0022-3727/46/39/395301
33. Wang C-M, Genc A, Cheng H, Pullan L, Baer DR, Bruemmer SM (2014) In-Situ TEM visualization of vacancy injection and chemical partition during oxidation of Ni–Cr nanoparticles. Sci Rep 4(1):3683. https://doi.org/10.1038/srep03683
34. Wu J, Gao W, Wen J, Miller DJ, Lu P, Zuo J-M, Yang H (2015) Growth of Au on Pt icosahedral nanoparticles revealed by low-dose in situ TEM. Nano Lett 15(4):2711–2715. https://doi.org/10.1021/acs.nanolett.5b00414
35. Liu Q, Zou R, Wu J, Xu K, Lu A, Bando Y, Golberg D, Hu J (2015) Molten Au/Ge alloy migration in Ge nanowires. Nano Lett 15(5):2809–2816. https://doi.org/10.1021/acs.nanolett.5b01144

36. Cheng F, Lian L, Li L, Rao J, Li C, Qi T, Zhang Z, Zhang J, Gao Y (2019) Hybrid growth modes of PbSe nanocrystals with oriented attachment and grain boundary migration. Adv Sci 6(9):1802202. https://doi.org/10.1002/advs.201802202
37. Wang ZL (2000) Transmission electron microscopy of shape-controlled nanocrystals and their assemblies. J Phys Chem B 104(6):1153–1175. https://doi.org/10.1021/jp993593c
38. Vitos L, Ruban AV, Skriver HL, Kollár J (1998) The surface energy of metals. Surf Sci 411(1):186–202. https://doi.org/10.1016/S0039-6028(98)00363-X
39. Stensgaard I, Feidenhans'l R, Sørensen J (1983) Surface relaxation of Cu (110): an ion scattering investigation. Surf Sci 128(2–3):281–293. https://doi.org/10.1016/S0039-6028(83)80032-6
40. Jayanthi CS, Tosatti E, Fasolino A, Pietronero L (1985) Multilayer relaxation and melting of a metal surface. Surf Sci 152–153:155–161. https://doi.org/10.1016/0039-6028(85)90139-6
41. Statiris P, Lu HC, Gustafsson T (1994) Temperature dependent sign reversal of the surface contraction of Ag(111). Phys Rev Lett 72(22):3574–3577. https://doi.org/10.1103/PhysRevLett.72.3574
42. Ding Y, Fan F, Tian Z, Wang ZL (2009) Sublimation-induced shape evolution of silver cubes. Small 5(24):2812–2815. https://doi.org/10.1002/smll.200901189
43. He L-B, Zhang L, Tan X-D, Tang L-P, Xu T, Zhou Y-L, Ren Z-Y, Wang Y, Teng C-Y, Sun L-T, Nie J-F (2017) Surface energy and surface stability of Ag nanocrystals at elevated temperatures and their dominance in sublimation-induced shape evolution. Small 13(27):1700743. https://doi.org/10.1002/smll.201700743
44. Tolman RC (1949) The effect of droplet size on surface tension. J Chem Phys 17(3):333–337. https://doi.org/10.1063/1.1747247
45. Lu HM, Jiang Q (2004) Size-dependent surface energies of nanocrystals. J Phys Chem B 108(18):5617–5619. https://doi.org/10.1021/jp0366264
46. Xiong S, Qi W, Cheng Y, Huang B, Wang M, Li Y (2011) Modeling size effects on the surface free energy of metallic nanoparticles and nanocavities. Phys Chem Chem Phys 13(22):10648–10651. https://doi.org/10.1039/c0cp02102d
47. Medasani B, Park YH, Vasiliev I (2007) Theoretical study of the surface energy, stress, and lattice contraction of silver nanoparticles. Phys Rev B 75(23):235436. https://doi.org/10.1103/PhysRevB.75.235436
48. Yao Y, Wei Y, Chen S (2015) Size effect of the surface energy density of nanoparticles. Surf Sci 636:19–24. https://doi.org/10.1016/j.susc.2015.01.016
49. Sambles JR, Skinner LM, Lisgarten ND, Blackman M (1970) An electron microscope study of evaporating small particles: the Kelvin equation for liquid lead and the mean surface energy of solid silver. Proceed Roy Soc Lond A Math Phys Sci 318(1535):507–522. https://doi.org/10.1098/rspa.1970.0157
50. Blackman M, Sambles J (1970) Melting of very small particles during evaporation at constant temperature. Nature 226(5249):938–938. https://doi.org/10.1038/226938a0
51. He L-B, Zhang L, Tang L-P, Sun J, Zhang Q-B, Sun L-T (2018) Novel behaviors/properties of nanometals induced by surface effects. Materials Today Nano 1:8–21. https://doi.org/10.1016/j.mtnano.2018.04.006
52. Cheng F, Lian L, Li L, Rao J, Li C, Qi T, Cheng Y, Zhang Z, Zhang J, Wang J, Gao Y (2020) Sublimation and related thermal stability of PbSe nanocrystals with effective size control evidenced by in situ transmission electron microscopy. Nano Energy 75:104816. https://doi.org/10.1016/j.nanoen.2020.104816
53. Golberg D, Costa PMFJ, Wang M-S, Wei X, Tang D-M, Xu Z, Huang Y, Gautam UK, Liu B, Zeng H, Kawamoto N, Zhi C, Mitome M, Bando Y (2012) Nanomaterial engineering and property studies in a transmission electron microscope. Adv Mater 24(2):177–194. https://doi.org/10.1002/adma.201102579
54. Regan B, Aloni S, Ritchie R, Dahmen U, Zettl A (2004) Carbon nanotubes as nanoscale mass conveyors. Nature 428(6986):924–927. https://doi.org/10.1038/nature02496
55. Svensson K, Olin H, Olsson E (2004) Nanopipettes for metal transport. Phys Rev Lett 93(14):145901. https://doi.org/10.1103/PhysRevLett.93.145901

56. Golberg D, Costa PM, Mitome M, Hampel S, Haase D, Mueller C, Leonhardt A, Bando Y (2007) Copper-filled carbon nanotubes: Rheostatlike behavior and femtogram copper mass transport. Adv Mater 19(15):1937–1942. https://doi.org/10.1002/adma.200700126
57. Huang JY, Lo Y-C, Niu JJ, Kushima A, Qian X, Zhong L, Mao SX, Li J (2013) Nanowire liquid pumps. Nat Nanotechnol 8(4):277–281. https://doi.org/10.1038/nnano.2013.41
58. Kim K, Jensen K, Zettl A (2009) Tuning nanoelectromechanical resonators with mass migration. Nano Lett 9(9):3209–3213. https://doi.org/10.1021/nl901449w
59. Jensen K, Kim K, Zettl A (2008) An atomic-resolution nanomechanical mass sensor. Nat Nanotechnol 3(9):533–537. https://doi.org/10.1038/nnano.2008.200
60. Begtrup GE, Gannett W, Yuzvinsky TD, Crespi VH, Zettl A (2009) Nanoscale reversible mass transport for archival memory. Nano Lett 9(5):1835–1838. https://doi.org/10.1021/nl803800c
61. Regan BC, Aloni S, Jensen K, Zettl A (2005) Surface-tension-driven nanoelectromechanical relaxation oscillator. Appl Phys Lett 86(12):123119. https://doi.org/10.1063/1.1887827
62. Dong T, Zhang L, Zhang NBJ (2007) Nanorobotic spot welding: controlled metal deposition with attogram precision from copper-filled carbon nanotubes. Nano Lett 7(1):58–63. https://doi.org/10.1021/nl061980+
63. Park G-S, Kim YB, Park SY, Li XS, Heo S, Lee M-J, Chang M, Kwon JH, Kim M, Chung U-I (2013) In situ observation of filamentary conducting channels in an asymmetric Ta_2O_{5-x}/TaO_{2-x} bilayer structure. Nat Commun 4(1):1–9. https://doi.org/10.1038/ncomms3382
64. Huang JY, Zhong L, Wang CM, Sullivan JP, Xu W, Zhang LQ, Mao SX, Hudak NS, Liu XH, Subramanian A, Fan H, Qi L, Kushima A, Li J (2010) In situ observation of the electrochemical lithiation of a single SnO_2 nanowire electrode. Science 330(6010):1515–1520. https://doi.org/10.1126/science.1195628
65. Celano U, Goux L, Belmonte A, Opsomer K, Franquet A, Schulze A, Detavernier C, Richard O, Bender H, Jurczak M, Vandervorst W (2014) Three-dimensional observation of the conductive filament in nanoscaled resistive memory devices. Nano Lett 14(5):2401–2406. https://doi.org/10.1021/nl500049g
66. Zhang Q, Yin K, Dong H, Zhou Y, Tan X, Yu K, Hu X, Xu T, Zhu C, Xia W (2017) Electrically driven cation exchange for in situ fabrication of individual nanostructures. Nat Commun 8(1):1–7. https://doi.org/10.1038/ncomms14889
67. Sagel A, Wanderka N, Wunderlich RK, Schubert-Bischoff P, Fecht HJ (1997) Early stages of solid-state amorphization reaction during mechanical alloying of a multicomponent Zr-powder mixture. Scripta Mater 38(1):163–169. https://doi.org/10.1016/S1359-6462(97)00408-9
68. Lucadamo G, Barmak K, Carpenter DT, Rickman JM (2001) Microstructure evolution during solid state reactions of Nb/Al multilayers. Acta Mater 49(14):2813–2826. https://doi.org/10.1016/S1359-6454(01)00176-8
69. Wang L, Qin XY (2003) The effect of mechanical milling on the formation of nanocrystalline Mg_2Si through solid-state reaction. Scr Mater 49(3):243–248. https://doi.org/10.1016/S1359-6462(03)00241-0
70. Fashandi H, Lai CC, Dahlqvist M, Lu J, Rosen J, Hultman L, Greczynski G, Andersson M, Lloyd Spetz A, Eklund P (2017) Ti_2Au_2C and $Ti_3Au_2C_2$ formed by solid state reaction of gold with Ti_2AlC and Ti_3AlC_2. Chem Commun 53(69):9554–9557. https://doi.org/10.1039/c7cc04701k
71. Kim G, Lee H, Kim J, Roh JW, Lyo I, Kim B-W, Lee KH, Lee W (2017) Up-scaled solid state reaction for synthesis of doped Mg_2Si. Scr Mater 128:53–56. https://doi.org/10.1016/j.scriptamat.2016.10.010
72. Mei S, He L, Wu X, Sun J, Wang B, Xiong X, Sun L (2014) Dynamic investigation of interface atom migration during heterostructure nanojoining. Nanoscale 6(1):405–411. https://doi.org/10.1039/c3nr03911k
73. Qian F, Gradečak S, Li Y, Wen C-Y, Lieber CM (2005) Core/multishell nanowire heterostructures as multicolor, high-efficiency light-emitting diodes. Nano Lett 5(11):2287–2291. https://doi.org/10.1021/nl051689e

74. Liang LH, Li B (2006) Size-dependent thermal conductivity of nanoscale semiconducting systems. Phys Rev B 73(15):153303. https://doi.org/10.1103/PhysRevB.73.153303
75. Westover T, Jones R, Huang JY, Wang G, Lai E, Talin AA (2009) Photoluminescence, thermal transport, and breakdown in Joule-Heated GaN nanowires. Nano Lett 9(1):257–263. https://doi.org/10.1021/nl802840w
76. Chen Y, Li Y, Ran G, Wu L, Ye C, Han Q, Wang H, Du H (2020) In-situ TEM observation of the evolution of dislocation loops and helium bubbles in a pre helium irradiated FeCrAl alloy during annealing. Prog Nucl Energy 129:103502. https://doi.org/10.1016/j.pnucene.2020.103502
77. Gatalo M, Ruiz-Zepeda F, Hodnik N, Dražić G, Bele M, Gaberšček M (2019) Insights into thermal annealing of highly-active $PtCu_3$/C oxygen reduction reaction electrocatalyst: an in-situ heating transmission electron microscopy study. Nano Energy 63:103892. https://doi.org/10.1016/j.nanoen.2019.103892
78. Meng S, Wu J, Zhao L, Zheng H, Jia S, Hu S, Meng W, Pu S, Zhao D, Wang J (2018) Atomistic Insight into the Redox Reactions in Fe/Oxide core-shell nanoparticles. Chem Mater 30(20):7306–7312. https://doi.org/10.1021/acs.chemmater.8b03679
79. Roy R, Hill VG, Osborn EF (1952) Polymorphism of Ga_2O_3 and the system Ga_2O_3–H_2O. J Am Chem Soc 74(3):719–722. https://doi.org/10.1021/ja01123a039
80. Cora I, Fogarassy Z, Fornari R, Bosi M, Rečnik A, Pécz B (2020) In situ TEM study of $\kappa \rightarrow \beta$ and $\kappa \rightarrow \gamma$ phase transformations in Ga_2O_3. Acta Mater 183:216–227. https://doi.org/10.1016/j.actamat.2019.11.019
81. Béché A, Rouvière JL, Clément L, Hartmann JM (2009) Improved precision in strain measurement using nanobeam electron diffraction. Appl Phys Lett 95(12):123114. https://doi.org/10.1063/1.3224886
82. Meyer T, Kressdorf B, Roddatis V, Hoffmann J, Jooss C, Seibt M (2021) Phase Transitions in a perovskite thin film studied by environmental in situ heating nano-beam electron diffraction. Small Methods 5(9):2100464. https://doi.org/10.1002/smtd.202100464
83. Tang L, Wu W, He L, Yu K, Xu T, Zhang Q, Zhang L, Sun L (2019) Novel interface in CuAg nanostructure induced by size effect. J Phys Chem Lett 10(8):1973–1980. https://doi.org/10.1021/acs.jpclett.9b00484
84. Ni Y, Kan C, He L, Zhu X, Jiang M, Shi D (2019) Alloyed Au-Ag nanorods with desired plasmonic properties and stability in harsh environments. Photon Res 7(5):558–565. https://doi.org/10.1364/prj.7.000558
85. Shi L, He L, Shangguan L, Zhou Y, Wang B, Zhang L, Yang Y, Teng C, Sun L (2022) Revealing the phase segregation and evolution dynamics in binary nanoalloys via electron beam-assisted ultrafast heating and cooling. ACS Nano 16(1):921–929. https://doi.org/10.1021/acsnano.1c08500
86. Yan Y, Du JS, Gilroy KD, Yang D, Xia Y, Zhang H (2017) Intermetallic nanocrystals: syntheses and catalytic applications. Adv Mater 29(14):1605997. https://doi.org/10.1002/adma.201605997
87. Chung DY, Jun SW, Yoon G, Kwon SG, Shin DY, Seo P, Yoo JM, Shin H, Chung Y-H, Kim H, Mun BS, Lee K-S, Lee N-S, Yoo SJ, Lim D-H, Kang K, Sung Y-E, Hyeon T (2015) Highly durable and active PtFe nanocatalyst for electrochemical oxygen reduction reaction. J Am Chem Soc 137(49):15478–15485. https://doi.org/10.1021/jacs.5b09653
88. Kuttiyiel KA, Sasaki K, Su D, Wu L, Zhu Y, Adzic RR (2014) Gold-promoted structurally ordered intermetallic palladium cobalt nanoparticles for the oxygen reduction reaction. Nat Commun 5(1):5185. https://doi.org/10.1038/ncomms6185
89. Xiong Y, Yang Y, Joress H, Padgett E, Gupta U, Yarlagadda V, Agyeman-Budu DN, Huang X, Moylan TE, Zeng R, Kongkanand A, Escobedo FA, Brock JD, DiSalvo FJ, Muller DA, Abruña HD (2019) Revealing the atomic ordering of binary intermetallics using in situ heating techniques at multilength scales. Proc Natl Acad Sci 116(6):1974. https://doi.org/10.1073/pnas.1815643116
90. Sun Y, Liu Y, Truong TT, Ren Y (2012) Thermal transformation of δ-MnO_2 nanoflowers studied by in-situ TEM. Sci China Chem 55(11):2346–2352. https://doi.org/10.1007/s11426-012-4688-5

91. Zhang L, Feng Q, Nie A, Liu J, Wang H, Fang Y (2014) *In situ* study of thermal stability of copper oxide nanowires at anaerobic environment. J Nanomater 2014:91. https://doi.org/10.1155/2014/670849
92. Wu J, Liu X, Bi H, Song Y, Wang C, Cao Q, Liu Z, Wang M, Che R (2016) Microwave sintering and in-situ transmission electron microscopy heating study of $Li_{1.2}(Mn_{0.53}Co_{0.27})O_2$ with improved electrochemical performance. J Power Sources 326:104–111. https://doi.org/10.1016/j.jpowsour.2016.06.102
93. Nam K-W, Bak S-M, Hu E, Yu X, Zhou Y, Wang X, Wu L, Zhu Y, Chung K-Y, Yang X-Q (2013) Combining in situ synchrotron x-ray diffraction and absorption techniques with transmission electron microscopy to study the origin of thermal instability in overcharged cathode materials for lithium-ion batteries. Adv Func Mater 23(8):1047–1063. https://doi.org/10.1002/adfm.201200693
94. Schwarz RB, Johnson WL (1983) Formation of an amorphous alloy by solid-state reaction of the pure polycrystalline metals. Phys Rev Lett 51(5):415–418. https://doi.org/10.1103/PhysRevLett.51.415
95. Holloway K, Sinclair R (1987) Amorphous Ti–Si alloy formed by interdiffusion of amorphous Si and crystalline Ti multilayers. J Appl Phys 61(4):1359–1364. https://doi.org/10.1063/1.338114
96. Si O, Kouzaki T, Yoshida T, Sinclair R (1991) Interface microstructure of titanium thin-film/silicon single-crystal substrate correlated with electrical barrier heights. J Appl Phys 70(2):827–832. https://doi.org/10.1063/1.349641
97. Konno TJ, Sinclair R (1992) Crystallization of silicon in aluminium/amorphous-silicon multilayers. Philos Mag B 66(6):749–765. https://doi.org/10.1080/13642819208220126
98. Konno TJ, Sinclair R (1995) Metal-mediated crystallization of amorphous silicon in silicon-silver layered systems. Philos Mag B 71(2):163–178. https://doi.org/10.1080/01418639508240304
99. Min KH, Sinclair R, Park IS, Kim ST, Chung UI (2005) Crystallization behaviour of ALD-Ta2O5 thin films: the application of in-situ TEM. Phil Mag 85(18):2049–2063. https://doi.org/10.1080/14786430500036546
100. Danev R, Yanagisawa H, Kikkawa M (2019) Cryo-electron microscopy methodology: current aspects and future directions. Trends Biochem Sci 44(10):837–848. https://doi.org/10.1016/j.tibs.2019.04.008
101. Wang L, Han X, Liu P, Yue Y, Zhang Z, Ma E (2010) In situ observation of dislocation behavior in nanometer grains. Phys Rev Lett 105(13):135501. https://doi.org/10.1103/PhysRevLett.105.135501
102. Taheri ML, Stach EA, Arslan I, Crozier PA, Kabius BC, LaGrange T, Minor AM, Takeda S, Tanase M, Wagner JB, Sharma R (2016) Current status and future directions for in situ transmission electron microscopy. Ultramicroscopy 170:86–95. https://doi.org/10.1016/j.ultramic.2016.08.007
103. Miller B, Pakzad A, Mick S (2019) Real-time electron counting for continuous TEM imaging of sensitive samples. Microsc Microanal 25(S2):1718–1719. https://doi.org/10.1017/s1431927619009322
104. Idrobo JC, Zhou W (2017) A short story of imaging and spectroscopy of two-dimensional materials by scanning transmission electron microscopy. Ultramicroscopy 180:156–162. https://doi.org/10.1016/j.ultramic.2017.02.002
105. Zhang B, Wang J, Wu B, Guo XW, Wang YJ, Chen D, Zhang YC, Du K, Oguzie EE, Ma XL (2018) Unmasking chloride attack on the passive film of metals. Nat Commun 9(1):2559. https://doi.org/10.1038/s41467-018-04942-x
106. Winterstein JP, Lin PA, Sharma R (2015) Temperature calibration for in situ environmental transmission electron microscopy experiments. Microsc Microanal 21(6):1622–1628. https://doi.org/10.1017/s1431927615015196
107. Jiang Y, Zhang Z, Yuan W, Zhang X, Wang Y, Zhang Z (2018) Recent advances in gas-involved in situ studies via transmission electron microscopy. Nano Res 11(1):42–67. https://doi.org/10.1007/s12274-017-1645-9

108. Liao H-G, Zheng H (2016) Liquid cell transmission electron microscopy. Annu Rev Phys Chem 67(1):719–747. https://doi.org/10.1146/annurev-physchem-040215-112501
109. Fernando JFS, Zhang C, Firestein KL, Golberg D (2017) Optical and optoelectronic property analysis of nanomaterials inside transmission electron microscope. Small 13(45):1701564. https://doi.org/10.1002/smll.201701564
110. Song C, Yang S, Li X, Li X, Feng J, Pan A, Wang W, Xu Z, Bai X (2019) Optically manipulated nanomechanics of semiconductor nanowires. Chin Phys B 28(5):054204. https://doi.org/10.1088/1674-1056/28/5/054204
111. Zhu S, Fu J, Li H, Zhu L, Hu Y, Xia W, Zhang X, Peng Y, Zhang J (2018) Direct observation of magnetocrystalline anisotropy tuning magnetization configurations in uniaxial magnetic nanomaterials. ACS Nano 12(4):3442–3448. https://doi.org/10.1021/acsnano.8b00058
112. Du H, Zhao X, Rybakov FN, Borisov AB, Wang S, Tang J, Jin C, Wang C, Wei W, Kiselev NS, Zhang Y, Che R, Blügel S, Tian M (2018) Interaction of individual skyrmions in a nanostructured cubic chiral magnet. Phys Rev Lett 120(19):197203. https://doi.org/10.1103/PhysRevLett.120.197203